HHS Public Access

Author manuscript

Nano Lett. Author manuscript; available in PMC 2022 June 09.

Published in final edited form as:

Nano Lett. 2021 June 09; 21(11): 4692–4699. doi:10.1021/acs.nanolett.1c00895.

Ultrasmall Porous Silica Nanoparticles with Enhanced Pharmacokinetics for Cancer Theranostics

Carolina A. Ferreira[∇],
Department of Biomedical Engineering, University of Wisconsin — Madison, Madison, Wisconsin 53705, United States

Shreya Goel[∇],
Materials Science & Engineering, University of Wisconsin — Madison, Madison, Wisconsin 53705, United States

Emily B. Ehlerding,
Medical Physics, University of Wisconsin — Madison, Madison, Wisconsin 53705, United States

Zachary T. Rosenkrans,
Pharmaceutical Sciences, University of Wisconsin — Madison, Madison, Wisconsin 53705, United States

Dawei Jiang,
Radiology, University of Wisconsin — Madison, Madison, Wisconsin 53705, United States

Tuanwei Sun,
Radiology, University of Wisconsin — Madison, Madison, Wisconsin 53705, United States

Eduardo Aluicio-Sarduy,
Medical Physics, University of Wisconsin — Madison, Madison, Wisconsin 53705, United States

Jonathan W. Engle,
Medical Physics, University of Wisconsin — Madison, Madison, Wisconsin 53705, United States

Dalong Ni,
Radiology, University of Wisconsin — Madison, Madison, Wisconsin 53705, United States

Weibo Cai

Corresponding Authors **Dalong Ni** — *Radiology, University of Wisconsin — Madison, Madison, Wisconsin 53705, United States;* Present Address: D.N.: Department of Orthopedics, Shanghai Key Laboratory for Prevention and Treatment of Bone and Joint Diseases, Shanghai Institute of Traumatology and Orthopedics, Ruijin Hospital, Shanghai Jiao Tong University School of Medicine, Shanghai 200025, P. R. China.; ndl12353@rjh.com.cn, ***Weibo Cai***— Department of Biomedical Engineering, Materials Science & Engineering, Medical Physics, Pharmaceutical Sciences, and Radiology, University of Wisconsin — Madison, Madison, Wisconsin 53705, United States; wcai@uwhealth.org.

[∇]C.A.F. and S.G. contributed equally. The manuscript was written through contributions of all authors. All authors have given approval to the final version of the manuscript.

Notes

The authors declare the following competing financial interest(s): Weibo Cai is a scientific advisor, stockholder, and grantee of Focus-X Therapeutics, Inc. All other authors declare that they have no conflict of interest.

ASSOCIATED CONTENT

Supporting Information

The Supporting Information is available free of charge at https://pubs.acs.org/doi/10.1021/acs.nanolett.1c00895.

Experimental section and methods as well as supplementary figures on nanoparticle characterization, radiolabeling stability, dosimetry studies, CLI, and toxicity studies (PDF)

Department of Biomedical Engineering, Materials Science & Engineering, Medical Physics, Pharmaceutical Sciences, and Radiology, University of Wisconsin — Madison, Madison, Wisconsin 53705, United States

Abstract

Theranostic nanoparticles hold the potential to greatly improve cancer management by providing personalized medicine. Although many theranostic nanoconstructs have been successful in preclinical studies, clinical translation is still hampered by their limited targeting capability and lack of successful therapeutic efficacy. We report the use of novel ultrasmall porous silica nanoparticles (UPSN) with enhanced *in vivo* pharmacokinetics such as high target tissue accumulation (12% ID/g in the tumor) and evasion from the reticuloendothelial system (RES) organs. Herein, UPSN is conjugated with the isotopic pair $^{90/86}$Y, enabling both noninvasive imaging as well as internal radiotherapy. *In vivo* PET imaging demonstrates prolonged blood circulation and excellent tumor contrast with ^{86}Y-DOTA-UPSN. Tumor-to-muscle and tumor-to-liver uptake values were significantly high (12.4 ± 1.7 and 1.5 ± 0.5, respectively), unprecedented for inorganic nanomaterials. ^{90}Y-DOTA-UPSN significantly inhibits tumor growth and increases overall survival, indicating the promise of UPSN for future clinical translation as a cancer theranostic agent.

Graphical Abstract

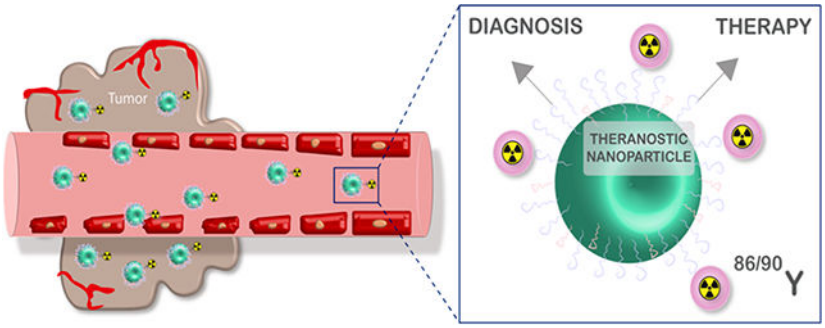

Keywords

Silica nanoparticles; Theranostics; Nanotheranostics; PET imaging; Yttrium-90; Yttrium-86

INTRODUCTION

Cancer theranostics refers to the combination of disease diagnosis and therapy. The theranostic strategy is essential for personalized cancer treatment; it aims at stratifying patients by likelihood to respond to a specific treatment, for early response monitoring as well as to predict efficacy.[1] In nuclear medicine, the theranostic approach combines diagnostic imaging and therapy using the same probe radiolabeled with either therapeutic or diagnostic radionuclides. Imaging is performed for dosimetry purposes and will determine the cumulative activity by extrapolating activity into dosage for different organs at different points in time. Therefore, the exactness of dosimetry highly depends on the quantitative

truthfulness of the imaging technique.[2] Many modalities are available for noninvasive molecular imaging. Compared to planar, single-photon emission computed tomography (SPECT) and bremsstrahlung imaging, positron emission tomography (PET) provides higher spatial resolution, sensitivity, and specificity resulting in a more accurate *in vivo* pharmacokinetic quantification.[1] For therapy, it is advantageous to use a radionuclide that is able to penetrate a greater depth of tissue and with high potential of causing radiation damage to the tumor tissue. Thus, high energy electrons (β^-) such as yttrium- 90 (^{90}Y) have been reported to have excellent therapeutic outcomes.[3] Since the theranostic approach cannot rely on the use of a same isotope for both diagnosis (positron emitter) and therapy (electron emitter), strategies are complicated by different radiolabeling procedures and potential dosimetric differences. The use of an isotopic theranostic pair is an extremely attractive option. As an example, yttrium-86 (^{86}Y) is a positron emitter (33%, $t_{1/2}$ = 14.7 h) that can be visualized with PET—with radiation dosage estimation—for subsequent therapy with its isotopically matched surrogate ^{90}Y.[4]

The combination of PET, radiotherapy, and nanotechnology poses a symbiotic relationship with mutual benefits arising from each component. Even though preclinical cancer nanobased approaches have yielded encouraging results,[5–13] the majority of the nanosystems still hold limited potential for future clinical translation due to high (>30% injected dose per gram) and long-term (>months) accumulation of nanoparticles in the reticuloendothelial system (RES) and, more importantly, lack of highly specific tumor targeting ability. It has been reported that an average of only 0.6% of injected dose per gram (ID/g) of the nanoparticle typically reaches tumor tissue through passive targeting.[14] To overcome the limited success of nanoparticles in oncology, it is paramount for researchers to discover systems that maximize tumor tissue accumulation without being retained in the RES organs.

To address that limitation, the complexity of finding the optimal nanoparticle size is of upmost importance for its *in vivo* behavior.[15,16] The recently Investigational New Drug (IND) approval of C-dots[17–19] (silica nanoparticle-based nano-constructs) have emerged as a promising research direction in that field.[20] While several attempts have been made to synthesize ultrasmall silica nanoplatforms, their size typically ranges from 25–50 nm, which is insufficient to evade RES uptake.[21,22] Our group has successfully synthesized a sub-15 nm porous silica nanoparticle with far superior pharmacokinetic characteristics, such as prolonged blood circulation, enhanced tumor uptake, and hepatic clearance.[23] After previous thorough characterization of our ultrasmall porous silica nanoparticle (UPSN),[23] herein, rather than focus on the pharmacokinetic characteristics of our nanotracer, we aimed at reporting an application study in which the ultrasmall porous silica nanoparticle (UPSN) is used as a nanocarrier for isotopic pair $^{86/90}$Y to allow a theranostic approach. This is the first time a silica nanoparticle is simultaneously radiolabeled with a theranostic isotopic pair, presents very high tumor uptake (12% ID/g), and allows dual-modality imaging for diagnosis and therapeutic monitoring, and it is used for dosimetry calculations of received organ dose estimates.

RESULTS AND DISCUSSION

Synthesis, Characterization, Surface Modification, and Radiolabeling of UPSN.

Precisely size-controlled nanoparticles were of upmost importance to achieve enhanced *in vivo* pharmacokinetics and allow a theranostic approach. UPSN synthesis was carried out through a variation of the method first described by Ma et al.[24] A major difference in our study was the modification of the synthesis procedure to finely tune the nanoparticle size between 12 and 15 nm to mimic biomacromolecules like antibodies, such that they were large enough to avoid rapid renal clearance while being small enough to afford longer blood circulation time and enhanced tumor uptake. Three key steps ensure exquisite control over particle size and morphology: (i) rapid hydrolysis of silica precursors, (ii) slow condensation and particle growth, and (iii) rapid quenching of particle growth by addition of the capping agent. A scheme of the synthesis process can be seen in Figure 1A. UPSN synthesis was achieved using tetramethyl orthosilica (TMOS) as the silane precursor hexadecyltrimethy-lammonium bromide (CTAB) as the structure-directing surfactant, ammonium hydroxide as the catalyst, and poly-ethylene glycol-silane (PEG-silane) as the reaction quencher, as previously reported.[24] TMOS was chosen as the silica precursor, instead of commonly used tetraethyl orthosilicate (TEOS), because of its faster condensation rate and higher hydrophilicity. Higher temperature treatment around 80 °C was found to be essential for particle monodispersity and stability.

Transmission electron microscopy (TEM) indicated the synthesis of the uniform porous structure of ~12.4 ± 2.4 nm in diameter (averaged over 100 nanoparticles; Figure S1A) which was confirmed by dynamic light scattering (DLS) measurements (approximately 13.5 nm, PDI = 0.1, Figure 1C). The conjugation of 1,4,7,10-tetraazacyclododecane-1,4,7,10-tetra- acetic acid (DOTA) chelator did not significantly affect the hydrodynamic size of the nanoparticles, as seen in Figure 1C. TEM images (Figure 1B) indicate the presence of nanoparticles with narrow size distribution with well-formed single pores and a small population with half-porous structures, potentially due to incomplete encapsulation of CTAB micelles by silica precursor. Nitrogen adsorption/desorption analysis was carried out on freeze-dried samples to evaluate their surface area and pore size distribution. Brunauer–Emmett– Teller (BET) analysis indicated a high specific surface area of ~505.77 m^2/g (inset of Figure S1C). The presence of pores was confirmed by BJH isotherm analysis, with a hysteresis loop characteristic of porous materials (Figure S1B). Pore diameters of 3.92 nm in average and a total pore volume of 0.49 cm^3/g was calculated (Figure S1C). Even though in this study we are not using an active-targeted drug delivery approach, our UPSNs can be potentially applied for that end due to its distinctive properties of high surface area, uniform pore size, large pore volume, with great capacity for drug loading combined with its optimal size distribution. Of note, UPSNs were found to be stable for at least 6 months under physiological conditions as previously reported by our group.[23] Other methods of characterization as well as a long-term structural stability of our UPSNs have also been reported in that paper.

For radiolabeling, aminated UPSN was first conjugated with DOTA chelator under alkaline conditions, as previously described.[25] The decay-corrected radiolabeling yield of UPSN-

DOTA with ^{86}Y is depicted in Figure 1D and 1E. Radiolabeling was time dependent with the highest value; obtained after 120 min of incubation. After PD-10 purification, the radiolabeling yield was found to be above 90%, as analyzed by iTLC. Radiolabeling stability studies in PBS and serum have also been performed (Table S3), and those results are in agreement with previously published studies using UPSN.[24]

In Vivo EPR-Mediated Tumor Targeting with ^{86}Y- DOTA-UPSN and *Ex Vivo* Studies.

After administration of 2–3 MBq of ^{86}Y-DOTA-UPSN in 4T1 tumor-bearing mice, serial positron emission tomography (PET) images were acquired at different points in time postinjection (for up to 48; h p.i.) (n = 5). Maximum intensity projection (MIP) PET images are presented in Figure 2A, and quantitative data ‘ obtained from region-of-interest (ROI) analysis of PET images is presented in Figure 2B. ^{86}Y-DOTA-UPSN exhibited prolonged blood circulation, with a significant signal in the blood pool at the first scan (25.5 ± 5.2% ID/g at 0.5 h p.i), which decreased slowly over time. Remarkably, the signal in the blood pool was still very high at 24 h p.i (10.7 ± 1.0% ID/ g), uncommon to most nanoparticles. A slight signal in the bladder can be seen at the first time points, most probably due; to the renal excretion of the smallest nanoparticles (<10 nm).

As expected for intravenously injected nanoprobes, a relatively ‘ moderate signal in the liver (14.8 ± 1.2% ID/g) and spleen (10.9 ± 1.9% ID/g) were observed at 0.5 h p.i. In contrast to the majority of radiolabeled nanoparticles that present an increasing and prolonged accumulation in RES organs, the radiolabeled UPSN had a steady decrease in the signal in the liver and spleen over the 48 h period of the study. This indicated clearance of ^{86}Y-DOTA-UPSN via the hepatobiliary pathway, as previously demonstrated in depth by our group.[23] It is known that sequestration of nanoparticles by the RES organs have hampered its clinical translation due to toxicity concerns,[26] and thus, renal-clearable nanoparticles have been proposed.[27–29] However, fast renal elimination can prevent sufficient target tissue accumulation.[30] We believe that, by achieving a nanoparticle size similar to that of antibodies (around 13 nm), we were able to design a nanoparticle that would be large enough to prevent fast renal clearance and small enough to resist early sequestration by the RES. This would ultimately lead to prolonged blood circulation and allow selective accumulation at the tumor site via EPR effect. In fact, the long-circulating and RES evading ^{86}Y-DOTA-UPSN showed a rapid tumor accumulation, attributed to the enhanced permeability and retention (EPR) effect that reached almost 12% ID/g. The tumor uptake increases with time (4.7 ± 0.5, 5.8 ± 1.0, 7.0 ± 1.1, 10.0 ± 1.3, and 10.9 ± 0.8% ID/g at 0.5, 2, 6, 12, and 48 h p.i., respectively) and peaked at 24 h p.i at 11.8 ± 1.1% ID/g, coinciding with blood pool clearance. Concomitant clearance of ^{86}Y-DOTA-UPSN from the RES organs and the rest of the body yielded excellent tumor-to- muscle tissue contrast (Figure 2D). It is known that inorganic nanoparticles accumulate early in RES organs, such as the liver, and herein, we aimed at diminishing that accumulation and increasing their clearance rate. In fact, the radiolabeled UPSN with enhanced tumor uptake and rapid hepatobiliary clearance yielded a tumor-to-liver ratio of 1.5 ± 0.5 at 48 h p.i. (Figure 2E), unprecedented for inorganic nanomaterials reported to date. We have also used the trapezoidal numerical integration method to estimate the area under the curve of the time-activity curves found by PET imaging, and $AUC_{0–48h}$ was found to be 489.2% ID g^{-1} h for the tumor tissue and

67.62% ID g^{-1} h for the muscle (Figure S2). Of note, in our previously published paper, an in depth pharmacokinetic study was carried out in which data regarding the elimination pathway and circulation half-life can be found.[23]

After the end of the imaging study, mice were euthanized and their main organs were collected for *ex vivo* biodistribution studies using a gamma counter (Figure 2C) ($n = 5$). Tumor uptake of ^{86}Y-DOTA-UPSN was 10.4 ± 0.8% ID/g. Organ uptake found in the *ex vivo* study matched and validated the tissue uptake values obtained from PET ROI analysis. This favorable pharmacokinetic profile provided confidence on the use of UPSNs labeled with ^{90}Y for the therapeutic studies.

As a proof-of-concept approach to generate valid organ and tumor dose estimation, we have extrapolated data from PET scans to an adult human female. Doses received by major organs can be seen in Figure S3A and are expressed as the total dose received by the organ, in which liver and spleen were the nontarget organs with the highest dose received, at 2.38 ± 0.96 and 1.89 ± 0.74 mSv/MBq, respectively. Tumor doses were also estimated (Figure S3B) using a dose-to-sphere model and are expressed as dose per gram of tissue. For example, for a 1 g sample of tumor, a dose of 0.20 ± 0.01 mGy/MBq was found.

Treatment Monitoring and *In Vivo* Therapeutic Efficacy of ^{90}Y-DOTA-UPSN.

Over the past few years, the isotope ^{90}Y has been exploited for therapeutic purposes.[31] Since ^{90}Y decays almost exclusively by emission of a beta-minus (β^-), its visualization through traditional noninvasive molecular imaging such as PET and SPECT is extremely difficult and complex.[32] On the bright side, due to the relatively high energy emission, ^{90}Y is a very efficient Cerenkov radiation emitter and can allow optical imaging through Cerenkov luminescence imaging (CLI),[33] as demonstrated by spectral emissions of ^{90}Y and ^{90}Y-DOTA-UPSN (Figure S4). In this study, CLI allowed the visualization of tumor uptake of the ^{90}Y-labeled nanotracer, with clear signals for up to 11 days (Figure 3A). This imaging modality could potentially serve to monitor treatment and contribute to therapeutic management.

Ex vivo imaging of the major organs (Figure 3B) and tumor tissues (Figure S5A) confirmed tumor uptake and the ability to monitor this nanotracer in the tumor through CLI. Radiant efficiency calculated from *in vivo* imaging (Figure S5B) verified tumor uptake with decreasing signal over time, attributed to radioactive decay. *Ex vivo* analysis of resected tissues confirmed that tumor uptake is significantly higher than the uptake found in any of the organs measured (Figure 3C). The combination of PET imaging with ^{86}Y-DOTA-UPSN, its dosimetric extrapolation, and the ability of tumor monitoring through CLI of ^{90}Y-DOTA-UPSN can provide invaluable complemental information and greatly assist in the decision of dosage before treatment as well as in the tumor response assessment throughout cancer therapy.

After administration of ~5.5 MBq of ^{90}Y-DOTA-UPSN, tumor growth was inhibited as tumor volumes were significantly smaller than all others starting as early as day 1 p.i. and throughout the rest of the study ($p < 0.05$, $n = 5$) (Figure 4A). From 1 day p.i. to 11 day p.i., the administration of the radionanotracer resulted in tumor regression of approximately

30%. None of the other groups presented tumor regression, and the tumors continued to grow exponentially, a difference that can be clearly seen when analyzing the collected tumor tissue (Figure S6). Even though complete tumor eradication was not achieved, we believe that the combination of early diagnosis, patient stratification, and reduced tumor volume can still be helpful for treatment management and potentially increase success of therapy. Furthermore, a few strategies can be employed to increase therapeutic efficacy in this case, such as the administration of multiple doses, the use of a different theranostic isotopic pair, or even the conjugation of a drug in the nanoplatform for synergistic effects. Further studies to investigate those possibilities are warranted. Importantly, no mice (0/5) injected with ^{90}Y-DOTA-UPSN had its tumor volume reach the end point criteria (>300% of initial), and 100% survival rate was found for that group at the end of the study. In contrast, 100% of the mice (5/5) that received either UPSN only or PBS only reached end points, and none of them were alive after day 15. Only 1 mouse in the group that received ^{90}Y-DOTA survived until the end of the study (Figure 4B). Thus, the value is evident of the therapeutic effect of ^{90}Y-DOTA-UPSN as well as its increased overall median survival.

Toxicity Evaluation.

Potential acute toxicities from ^{90}Y- labeled tracers were evaluated through tissue staining and measurement of relevant blood parameters. Histological staining of the major organs (Figure S7A) showed no overall toxicity or abnormal histopathological findings in any of the off-target organs for any of the groups except those injected with ^{90}Y-DOTA. In the ^{90}Y-DOTA group, all organs presented morphological abnormalities. Normal histopathology was found in the tumor for the PBS and UPSN alone groups, while for the animals administered with ^{90}Y-DOTA, some signs of necrosis could be observed. In comparison, for the animals administered with ^{90}Y-DOTA-UPSN, significant damage and large areas of necrosis (Figure S7B) can be seen, confirming antitumor effects. As body weight changes can be an indicative of certain toxicity, body weight measurements were collected every other day. Throughout the study, none of the groups presented body weights near the set end point, suggesting relatively low toxicity to administered agents (Figure S8). To evaluate more in depth the possible toxic effects on some of the major off-target organs, blood samples of all mice were collected at the end of the study, and we analyzed kidney and liver enzymes levels. For the kidney toxicity evaluation, levels of creatinine and blood urea nitrogen (BUN) were analyzed. For the evaluation of potential toxicity in the liver, blood levels of aspartate amino transferase (AST), alanine amino transferase (ALT), total bilirubin, and alkaline phosphatase (ALP) were studied. Results from the kidney and liver function studies revealed no statistical difference between values found for the PBS-treated group in comparison to any other groups, except those injected with ^{90}Y-DOTA (Figure 5). For that group, levels of AST, total bilirubin, ALP, and creatinine were altered, indicating a certain toxicity to ^{90}Y-DOTA. This data corroborates with H&E staining findings. The analyzed blood levels for the mice injected with ^{90}Y-DOTA-UPSN were not statistically different than those found in the PBS-injected group. However, complete blood count measurements demonstrated potential toxic effects of the radiotherapy treatments (Figure S9), as significant smaller absolute values of white blood cells, lymphocytes, and red blood cells were found for mice injected with ^{90}Y-DOTA-UPSN at day 15 p.i. when compared to those at day 0. This is probably due to increased circulation half-life of the nanotracer and relatively high-energy

beta of ^{90}Y that can travel relatively long distances in the smaller body of a mouse when compared to humans. Decreased absolute values of lymphocytes and red blood cells were also found for the ^{90}Y-DOTA injected group of mice, which also reflect that more radiosensitive tissues, such as the bone marrow, can present with toxic effects in animal models. Decreases in platelet counts were also noted for those groups. Further in-depth toxicity studies are needed to assess the reversibility of cytopenia and bone marrow potential detriment effects of the utilization of Y-90 as a therapeutic isotope in this scenario. Optimization of dosing regimens by using fractionated doses could possibly overcome these issues and will be investigated in future studies. In addition, because we can use dosimetry studies to calculate the absorbed dose in multiple organs before administering the UPSN with the therapeutic isotope, we warrant the possibility of managing the dose injected in a way to protect nontargeted tissue in a personalized manner.

CONCLUSION

In this study, we describe the use of the isotopic pair ^{86}Y/^{90}Y coupled with UPSN as a means to obtain a theranostic nanoconstruct. UPSNs were successfully synthesized and exhibited outstanding *in vivo* behavior, including super long circulation behavior with signals in the heart still found after 24 h. PET imaging, validated by an *ex vivo* biodistribution study, of ^{86}Y-labeled nanoparticles allowed the visualization of its rapid selective accumulation in the target tissue throughout the entire study. Noteworthily, the combination of long circulation and RES evasion allowed the achievement of a high target specific accumulation with tumor uptake reaching around 12% ID/g. Optimal size UPSNs also yielded unprecedented tumor- to-liver and tumor-to-muscle ratios of around 1.5 and 12, respectively. Administration of ^{90}Y-labeled UPSNs provided promising therapeutic results with significantly reduced tumor volumes when compared to the other groups from as early as day 1 after administration. While the therapeutic effects were insufficient to completely eliminate tumors, important therapeutic outcomes such as a significantly increased average survival were reported. In fact, 100% of animals injected with radiolabeled UPSNs were still alive at the end of the study (in comparison to 20% for those injected with ^{90}Y-DOTA and 0% for the other groups). In addition, its long-term monitoring could be assessed through CLI, and a dosimetric extrapolation of potential organ and tumor dose to an adult human female has been calculated. We have also demonstrated through several experiments that the radiolabeled nanoparticles had low levels of nontarget tissue toxicity. The use of a safe nanoparticle that can achieve high tumor accumulations provides a platform for imaging and therapy as well as permits dosimetry calculations that can have important implications for cancer treatment, patient stratification, and cancer management. Further studies are warranted to improve therapeutic efficacy and to investigate how $^{86/90}$Y-DOTA-UPSN can best integrate the current standard of care for cancer patients.

Supplementary Material

Refer to Web version on PubMed Central for supplementary material.

ACKNOWLEDGMENTS

This work was supported by the University of Wisconsin — Madison, the National Institutes of Health (P30CA014520), and the Brazilian Science Without Borders Program (SwB- CNPq).

ABBREVIATIONS

UPSN	ultrasmall porous silica nanoparticles
PET	positron emission tomography
ID/g	injected dose per gram
RES	reticuloendothelial system
CLI	Cerenkov luminescence imaging

REFERENCES

(1). Chen X; Wong STC Chapter 1 — Cancer Theranostics: An Introduction. In Cancer Theranostics, Chen X; Wong S, Eds.; Academic Press: Oxford, 2014; pp 3–8.

(2). Li T; Ao ECI; Lambert B; Brans B; Vandenberghe S; Mok GSP Quantitative Imaging for Targeted Radionuclide Therapy Dosimetry - Technical Review. Theranostics 2017, 7 (18), 4551–4565. [PubMed: 29158844]

(3). Hsieh TC; Wu YC; Sun SS; Yen KY; Kao CH Treating hepatocellular carcinoma with (90)Y-bearing microspheres: a review. Biomedicine 2016, 6 (4), 19. [PubMed: 27848114]

(4). Nayak TK; Brechbiel MW 86Y based PET radiopharmaceuticals: radiochemistry and biological applications. Med. Chem 2011, 7 (5), 380–388. [PubMed: 21711222]

(5). Song J; Yang X; Jacobson O; Huang P; Sun X; Lin L; Yan X; Niu G; Ma Q; Chen X Ultrasmall Gold Nanorod Vesicles with Enhanced Tumor Accumulation and Fast Excretion from the Body for Cancer Therapy. Adv. Mater 2015, 27 (33), 4910–7. [PubMed: 26198622]

(6). Fan W; Bu W; Shen B; He Q; Cui Z; Liu Y; Zheng X; Zhao K; Shi J Intelligent MnO2 Nanosheets Anchored with Upconversion Nanoprobes for Concurrent pH-/H2O2-Responsive UCL Imaging and Oxygen-Elevated Synergetic Therapy. Adv. Mater 2015, 27 (28), 4155–61. [PubMed: 26058562]

(7). Chen H; Wang GD; Chuang YJ; Zhen Z; Chen X; Biddinger P; Hao Z; Liu F; Shen B; Pan Z; Xie J Nanoscintillator-mediated X-ray inducible photodynamic therapy for in vivo cancer treatment. Nano Lett. 2015, 15 (4), 2249–56. [PubMed: 25756781]

(8). Chen F; Hong H; Goel S; Graves SA; Orbay H; Ehlerding EB; Shi S; Theuer CP; Nickles RJ; Cai W In Vivo Tumor Vasculature Targeting of CuS@MSN Based Theranostic Nanomedicine. ACS Nano 2015, 9 (4), 3926–34. [PubMed: 25843647]

(9). Hong H; Shi J; Yang Y; Zhang Y; Engle JW; Nickles RJ; Wang X; Cai W Cancer-targeted optical imaging with fluorescent zinc oxide nanowires. Nano Lett. 2011, 11 (9), 3744–50. [PubMed: 21823599]

(10). Yang K; Zhang S; Zhang G; Sun X; Lee ST; Liu Z Graphene in mice: ultrahigh in vivo tumor uptake and efficient photothermal therapy. Nano Lett. 2010, 10 (9), 3318–23. [PubMed: 20684528]

(11). Bardhan R; Chen W; Bartels M; Perez-Torres C; Botero MF; McAninch RW; Contreras A; Schiff R; Pautler RG; Halas NJ; Joshi A Tracking of multimodal therapeutic nanocomplexes targeting breast cancer in vivo. Nano Lett. 2010, 10 (12), 4920–8. [PubMed: 21090693]

(12). Jiang Y; Huang J; Xu C; Pu K Activatable polymer nanoagonist for second near-infrared photothermal immunotherapy of cancer. Nat. Commun 2021, 12 (1), 742. [PubMed: 33531498]

(13). Li J; Cui D; Jiang Y; Huang J; Cheng P; Pu K Near-Infrared Photoactivatable Semiconducting Polymer Nanoblockaders for Metastasis-Inhibited Combination Cancer Therapy. Adv. Mater. (Weinheim, Ger.) 2019, 31 (46), No. 1905091.

(14). Torrice M Does Nanomedicine Have a Delivery Problem? ACS Cent. Sci 2016, 2 (7), 434–7. [PubMed: 27504489]

(15). Barar J Bioimpacts of nanoparticle size: why it matters? Bioimpacts 2015, 5 (3), 113–5. [PubMed: 26457247]

(16). Hoshyar N; Gray S; Han H; Bao G The effect of nanoparticle size on in vivo pharmacokinetics and cellular interaction. Nanomedicine 2016, 11 (6), 673–92. [PubMed: 27003448]

(17). Burns AA; Vider J; Ow H; Herz E; Penate-Medina O; Baumgart M; Larson SM; Wiesner U; Bradbury M Fluorescent silica nanoparticles with efficient urinary excretion for nanomedicine. Nano Lett. 2009, 9 (1), 442–8. [PubMed: 19099455]

(18). Benezra M; Penate-Medina O; Zanzonico PB; Schaer D; Ow H; Burns A; DeStanchina E; Longo V; Herz E; Iyer S; Wolchok J; Larson SM; Wiesner U; Bradbury MS Multimodal silica nanoparticles are effective cancer-targeted probes in a model of human melanoma. J. Clin. invest 2011, 121 (7), 2768–80. [PubMed: 21670497]

(19). Phillips E; Penate-Medina O; Zanzonico PB; Carvajal RD; Mohan P; Ye Y; Humm J; Gonen M; Kalaigian H; Schoder H; Strauss HW; Larson SM; Wiesner U; Bradbury MS Clinical translation of an ultrasmall inorganic optical-PET imaging nanoparticle probe. Sci. Transl Med 2014, 6 (260), 260ra149.

(20). Longmire M; Choyke PL; Kobayashi H Clearance properties of nano-sized particles and molecules as imaging agents: considerations and caveats. Nanomedicine 2008, 3 (5), 703–17. [PubMed: 18817471]

(21). Wu M; Meng Q; Chen Y; Du Y; Zhang L; Li Y; Zhang L; Shi J Large-pore ultrasmall mesoporous organosilica nanoparticles: micelle/precursor co-templating assembly and nuclear-targeted gene delivery. Adv. Mater 2015, 27 (2), 215–22. [PubMed: 25423915]

(22). Zheng H; Tai CW; Su J; Zou X; Gao F Ultra-small mesoporous silica nanoparticles as efficient carriers for pH responsive releases of anti-cancer drugs. Dalton Trans 2015, 44 (46), 20186–92. [PubMed: 26535559]

(23). Goel S; Ferreira CA; Dogra P; Yu B; Kutyreff CJ; Siamof CM; Engle JW; Barnhart TE; Cristini V; Wang Z; Cai W Size-Optimized Ultrasmall Porous Silica Nanoparticles Depict Vasculature-Based Differential Targeting in Triple Negative Breast Cancer. Small 2019, 15 (46), No. 1903747.

(24). Ma K; Sai H; Wiesner U Ultrasmall sub-10 nm near-infrared fluorescent mesoporous silica nanoparticles. J. Am. Chem. Soc 2012, 134 (32), 13180–3. [PubMed: 22830608]

(25). Goel S; Chen F; Hong H; Valdovinos HF; Hernandez R; Shi S; Barnhart TE; Cai W VEGF(1)(2)(1)-conjugated mesoporous silica nanoparticle: a tumor targeted drug delivery system. ACS Appl Mater. Interfaces 2014, 6 (23), 216772–85.

(26). Kwon IK; Lee SC; Han B; Park K Analysis on the current status of targeted drug delivery to tumors. J. Controlled Release 2012, 164 (2), 108–14.

(27). Phillips E; Penate-Medina O; Zanzonico PB; Carvajal RD; Mohan P; Ye Y; Humm J; Gonen M; Kalaigian H; Schoder H; Strauss HW; Larson SM; Wiesner U; Bradbury MS Clinical translation of an ultrasmall inorganic optical-PET imaging nanoparticle probe. Sci. Transl. Med 2014, 6 (260), 260ra149.

(28). Huang J; Jiang Y; Li J; He S; Huang J; Pu K A Renal- Clearable Macromolecular Reporter for Near-Infrared Fluorescence Imaging of Bladder Cancer. Angew. Chem. Int. Ed 2020, 59 (11), 4415–4420.

(29). Huang J; Li J; Lyu Y; Miao Q; Pu K Molecular optical imaging probes for early diagnosis of drug-induced acute kidney injury. Nat. Mater 2019, 18 (10), 1133–1143. [PubMed: 31133729]

(30). Yu M; Xu J; Zheng J Renal Clearable Luminescent Gold Nanoparticles: From the Bench to the Clinic. Angew. Chem., Int. Ed 2019, 58 (13), 4112–4128.

(31). Goffredo V; Paradiso A; Ranieri G; Gadaleta CD Yttrium- 90 (90Y) in the principal radionuclide therapies: an efficacy correlation between peptide receptor radionuclide therapy, radio-

immunotherapy and transarterial radioembolization therapy. Ten years of experience (1999–2009). Crit Rev. Oncol Hematol 2011, 80 (3), 393–410. [PubMed: 21388824]

(32). Mitchell GS; Lloyd PNT; Cherry SR Cerenkov luminescence and PET imaging of (90)Y: capabilities and limitations in small animal applications. Phys. Med. Biol 2020, 65 (6), 065006. [PubMed: 32045899]

(33). Gill RK; Mitchell GS; Cherry SR Computed Cerenkov luminescence yields for radionuclides used in biology and medicine. Phys. Med. Biol 2015, 60 (11), 4263–80. [PubMed: 25973972]

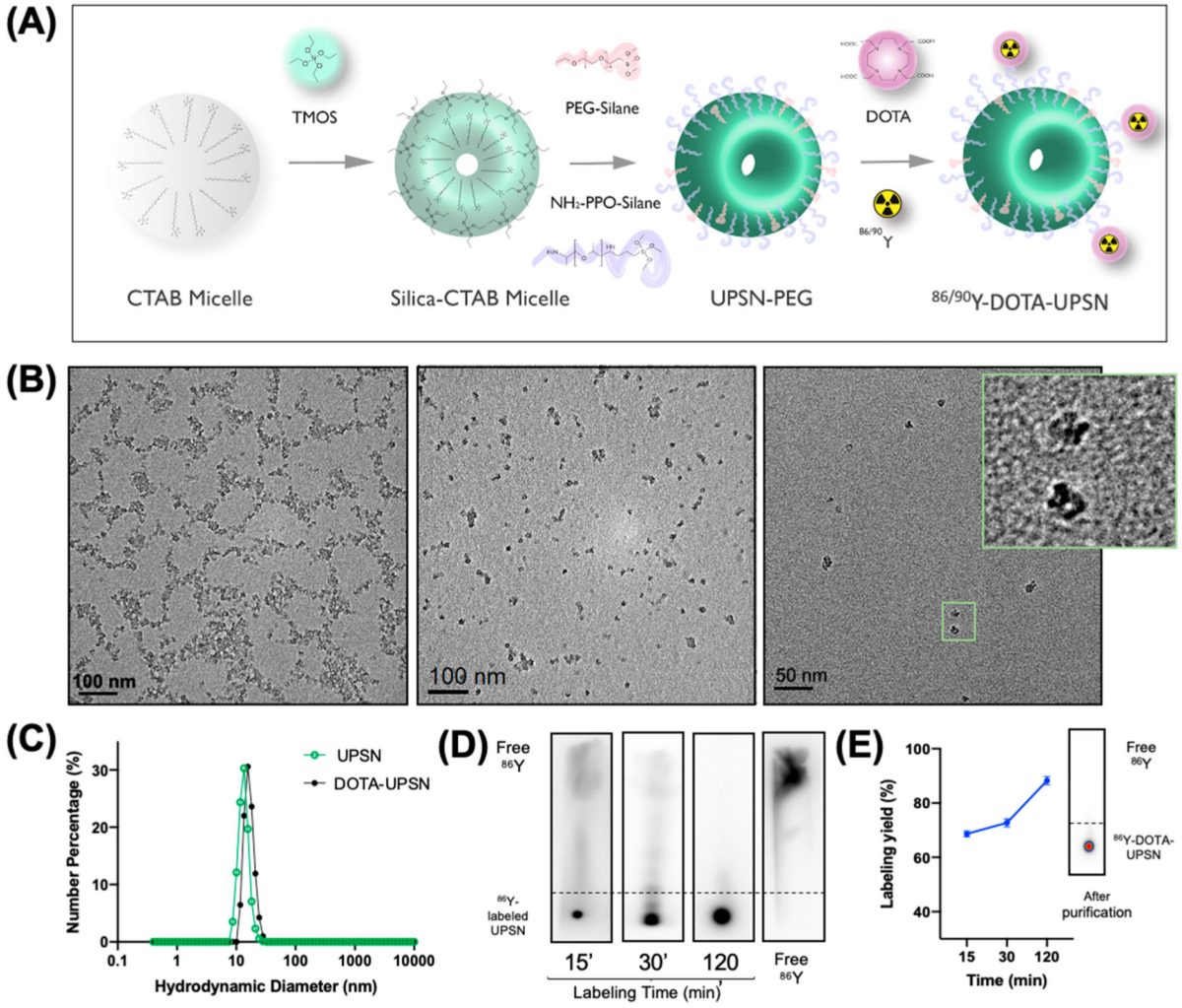

Figure 1.

Nanoparticle synthesis and characterization. (A) Schematic representation of the UPSN synthesis method. (B) Transmission electron microscopy (TEM) images of UPSN at different magnifications. The inset corresponds to a magnified image of individual nanoparticles. (C) Hydrodynamic diameters of UPSN and UPSN conjugated with DOTA chelator. (D, E) Radiolabeling studies of ^{86}Y-DOTA-UPSNs with (D) an autoradiograph of thin-layer chromatograms after different incubation time-points and (E) labeling yields as a function of incubation time. Insert in (E) is a representative iTLC of ^{86}Y-DOTA-UPSNs after PD-10 purification, depicting very high radiochemical yield with negligible migration of free isotope.

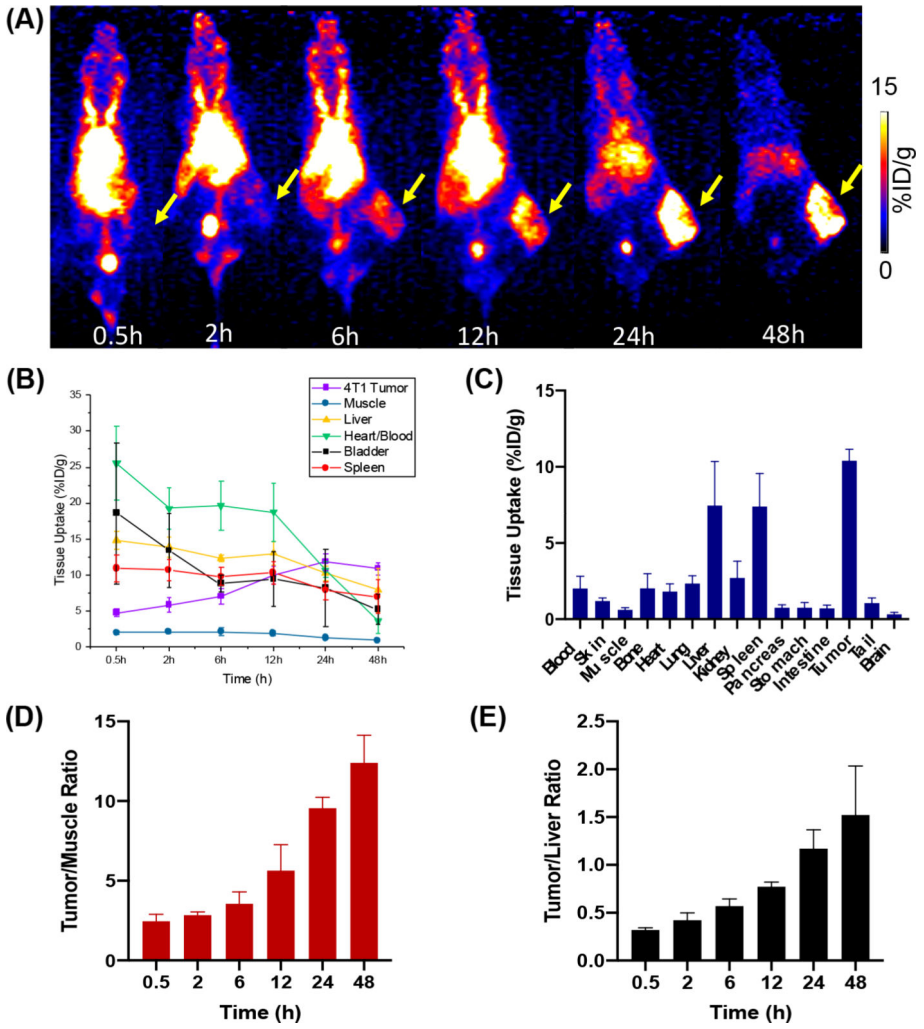

Figure 2.

In *vivo* PET imaging of 4T1 tumor-bearing mice with ^{86}Y-DOTA-UPSN. (A) Serial MIP PET images of 4T1 tumor-bearing mice injected with ^{86}Y-DOTA-UPSN ($n = 5$). Tumors are indicated with yellow arrows. (B) Time-activity curves of liver, muscle, blood pool, spleen, bladder, and tumor. (C) *Ex vivo* biodistribution performed after the last scan at 48 h p.i. (D) Tumor-to-muscle and (E) tumor-to-liver ratios obtained from the ROI analysis of PET images.

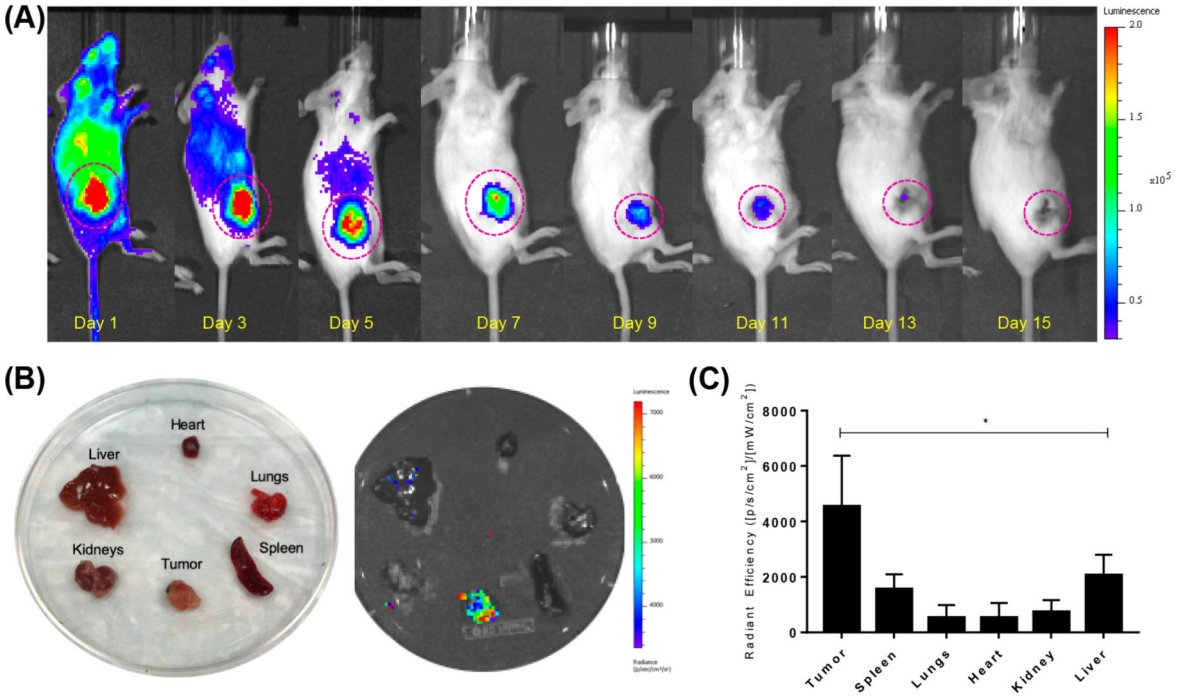

Figure 3.

Monitoring of ^{90}Y-DOTA-UPSN. (A) Long-term Cerenkov luminescence imaging of mice injected with ^{90}Y-DOTA-UPSN demonstrated tumor accumulation throughout a therapeutic study. (B) *Ex vivo* CLI of major organs confirmed high tumor uptake relative to other tissues. (C) Quantitave data of radiant efficiency of major organs calculated from *ex vivo* CLI. *Significantly higher ($p < 0.05$) than all the others investigated ($n = 5$).

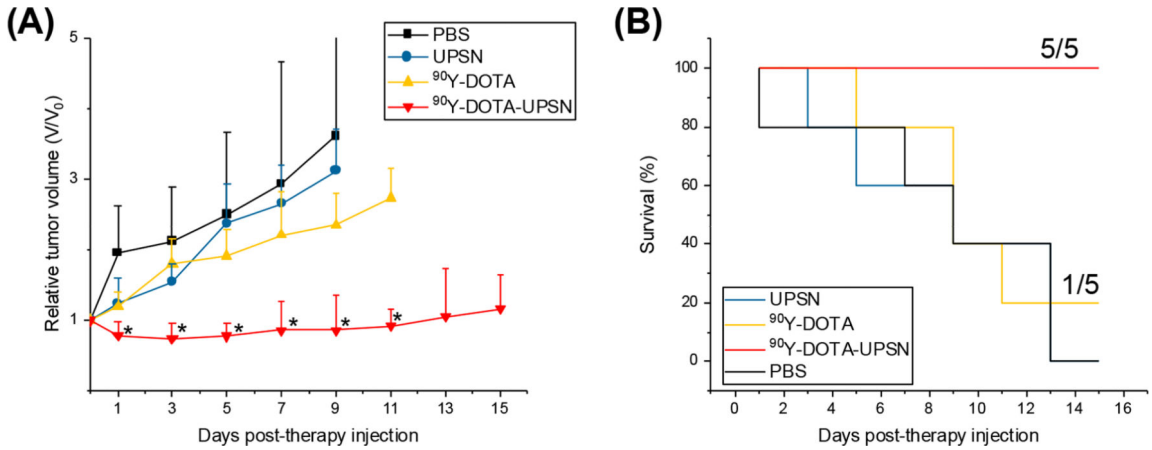

Figure 4.

Therapeutic studies for ^{90}Y-DOTA-UPSN. (A) Tumor growth curves. *Significantly smaller relative tumor volumes found for the group of mice injected with ^{90}Y-DOTA-UPSN when compared to all other groups ($p < 0.05$, $n = 5$). (B) Overall survival curve demonstrating significant extension in median survival in the group treated with ^{90}Y-DOTA-UPSN.

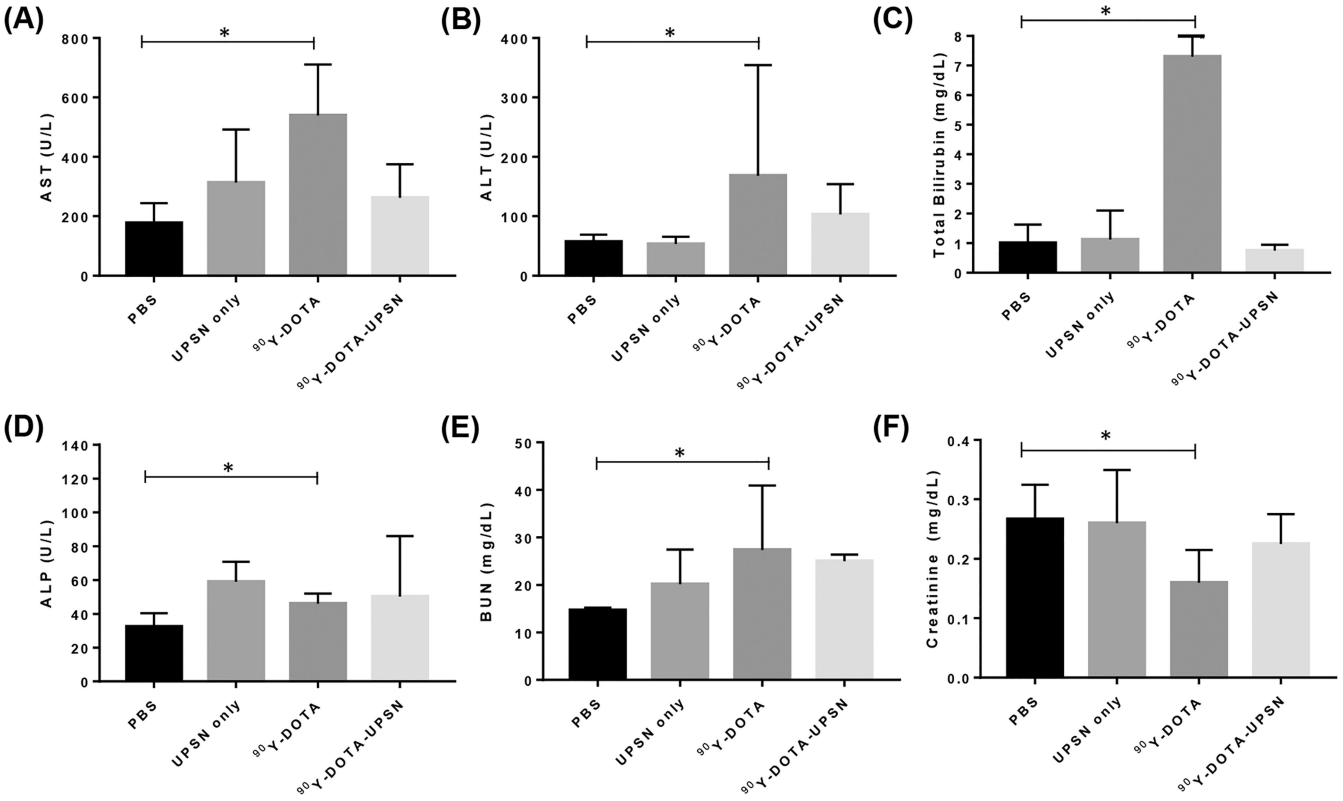

Figure 5.

Kidney and liver function tests. Serum values of (A) aspartate amino transferase (AST), (B) alanine amino transferase (ALT), (C) total bilirubin, (D) alkaline phosphatase (ALP), (E) blood urea nitrogen, and (F) creatinine collected at 15 days postinjection for all treatment groups. *Significantly different ($p < 0.05$, $n = 5$).